J. Synchrotron Rad. (1998). **5**, 1127–1129

Bronchography test studies at the angiography station of the VEPP-3 storage ring

V. I. Kondratyev, G. N. Kulipanov, M. V. Kuzin,* N. A. Mezentsev, S. I. Nesterov and V. F. Pinduyrin

Budker Institute of Nuclear Physics, 630090 Novosibirsk, Russia. E-mail: m.v.kuzin@inp.nsk.su

(*Received 4 August 1997; accepted 12 November 1997*)

The *K*-edge dichromography method was applied for preliminary bronchography test studies at the angiography station on the VEPP-3 storage ring. Images of xenon distribution over the test sample of Plexiglass were acquired. The obtained results demonstrate that thicknesses of xenon as small as 0.5 mm can be visualized.

Keywords: dichromography; bronchography; xenon.

1. Introduction

As shown by Rubenstein *et al.* (1995), the technique of digital subtraction angiography can be successfully applied for bronchography studies at the *K*-absorption edge of xenon. The necessity and significance of improvement of bronchography examinations were also revealed (Rubenstein *et al.*, 1995).

The existing angiography station at the Budker Institute of Nuclear Physics (Novosibirsk) is intended for experiments on dichromography imaging at the *K*-absorption edge of iodine (33.2 keV) (Kolesnikov *et al.*, 1995). The station uses synchrotron radiation from the 2 T wiggler installed on the VEPP-3 storage ring, and is equipped with a special double-beam X-ray monochromator and double one-coordinate X-ray detector.

In previous experiments, the station was used for testing the possibilities of visualization of the lymphatic system of live rats at the *K*-edge of iodine (Kolesnikov *et al.*, 1995). The present paper describes preliminary experiments on the visualization of xenon distribution over the test sample (phantom). The purpose of the experiments is to investigate the station capabilities for bronchography studies.

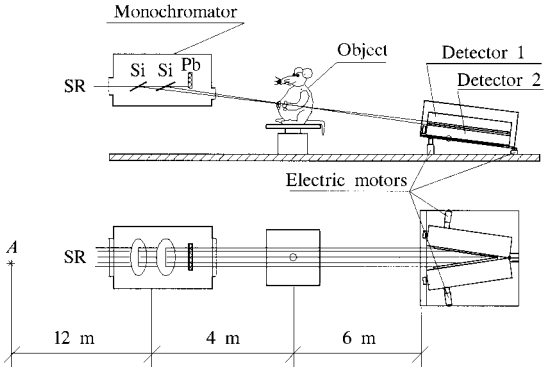

Figure 1
Schematic diagram of the angiography station.

2. Angiography station

The angiography station is schematically shown in Fig. 1. The main components of the station are the double one-coordinate X-ray detector, the object scanner and the double-beam X-ray monochromator.

The monochromator forms two wide (~10 cm width at the object position) monochromatic X-ray beams with energy just above and below that of the *K*-edge absorption of xenon (34.5 keV). The monochromatic beams intersect at the object location, then they diverge and are registered simultaneously by the double one-coordinate X-ray detector. Thus, we simultaneously obtain one horizontal line of the image at two X-ray quanta energies. The complete picture is obtained by moving the object vertically and line-by-line registration of the beams passing through the object.

The monochromator comprises two Si(100) crystals in Laue diffraction geometry with a 100 mm diameter, the entrance slit and the attenuator of the white synchrotron radiation beam (Barsukov *et al.*, 1991). The distance between the crystals can be changed in the range 30–50 mm, which provides the relative energy separation of the monochromatic beams in the range 6×10^{-3} to 10×10^{-3}. Depending on the entrance slit size, the relative energy spread of each beam can be in the range from 10^{-3} to 8×10^{-3}. The provided photon flux at the object location is about 10^8 photons s^{-1} mm^{-2} at a typical 100 mA current in the VEPP-3 storage ring.

The double one-coordinate X-ray detector (Dementiev *et al.*, 1989; Kolesnikov *et al.*, 1995, 1996) consists of two identical one-coordinate X-ray detectors. The detector design allows one to change its spatial resolution from 0.2 mm to 2 mm. Each one-coordinate detector has 128 separate scintillation counters based on photomultipliers (PMT-60) and $YAlO_3$(Ce) scintillators with 2 mm thickness and 40 ns decay time. The maximum counting rate of each detector channel is about 6–7 MHz, and the measured registration efficiency of the detector is about 90% (Kolesnikov *et al.*, 1996).

3. Experiment and results

For studying the method sensitivity to registration of Xe, a Plexiglass phantom with a xenon contamination inside was used (Fig. 2). The phantom contained several internal spaces with thicknesses of xenon from 5 mm down to 0.5 mm. In the experiment, the internal phantom cavity, after being firstly evacuated of air, was filled with xenon at a pressure of ~1 atm.

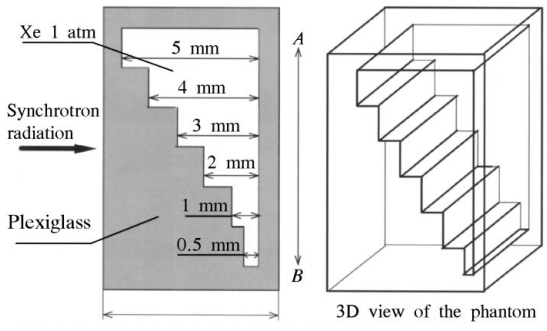

Figure 2
Schematic drawing of the phantom (*AB* is the direction of scanning in the experiment).

The monochromator was tuned to the *K*-absorption edge of xenon (34.5 keV); the relative energy separation of the monochromatic beams was about 1.25×10^{-2}. Due to a lack of space in the synchrotron radiation experimental hall, we were forced to intersect the monochromatic beams ahead of the phantom location. This meant that the beams passed through the phantom with different vertical coordinates. This fact, as well as a small relative inclination of the beamlines, was taken into account in the further processing of data and images. The typical number of registered photons in the experiments lay in the range 2×10^5 to 4×10^5 per detector channel. The reference lines without the phantom were registered, also at energies above and below the xenon *K*-edge, and were used for subsequent normalization of the lines acquired with the phantom.

The photon flux, I, passing through the phantom with xenon, can be written in the form

$$I^{\pm} = I_0 \exp(-\mu^{\pm}_{\rm Xe}\rho_{\rm Xe}d_{\rm Xe}) \exp(-\mu^{\pm}_{\rm P}\rho_{\rm P}d_{\rm P}),$$

where I_0 is the incident photon flux and μ, ρ and d are the mass absorption coefficient, density and thickness, respectively. Subscripts Xe and P correspond to xenon and Plexiglass, respectively, and the plus and minus superscripts correspond to the energies above and below the *K*-edge of xenon, respectively.

Therefore, the result of logarithmic subtraction is

$$R = \ln(I^+/I^-) = -(\Delta\mu\rho d)_{\rm Xe} + (\Delta\mu\rho d)_{\rm P},$$

where $\Delta\mu = \mu^+ - \mu^-$. Assuming that $\mu_{\rm P} = \text{constant}/E^n$, where E is the quanta energy, we can write

$$\Delta\mu_{\rm P} = -n\mu_{\rm P}\Delta E/E,$$

where $\Delta E/E$ is the relative energy separation of the beams.

The final expression for R can be written as

$$R = \ln(I^+/I^-) = -(\Delta\mu\rho d)_{\rm Xe} + n(\mu\rho d)_{\rm P}\Delta E/E.$$

In our case, $\Delta\mu_{\rm Xe} = 27.77\ \text{cm}^2\ \text{g}^{-1}$, $\rho_{\rm Xe} = 5.89 \times 10^{-3}\ \text{g cm}^{-3}$, $\mu_{\rm P} = 0.261\ \text{cm}^2\ \text{g}^{-1}$, $n = 0.827$, $\rho_{\rm P} = 1.2\ \text{g cm}^{-3}$ and $\Delta E/E = 1.25 \times 10^{-2}$. The values of the mass absorption coefficients are taken from Zapisov *et al.* (1975). The calculated and measured results are presented in Table 1. Differences between the calculated and measured R values may be due to two reasons:

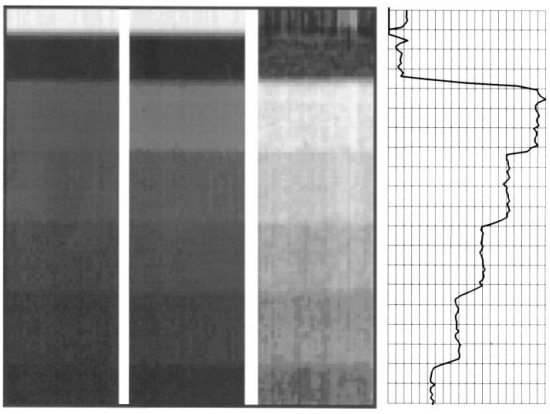

Figure 3
On the left-hand side, three X-ray images of the phantom with xenon: the usual X-ray images at the energy above (left) and below (middle) the *K*-edge of xenon, and the subtraction image (right). On the right-hand side, the xenon distribution curve in the phantom along the vertical direction.

Table 1
Calculated and measured results.

$d_{\rm Xe}$ (mm)	$d_{\rm P}$ (mm)	$-(\Delta\mu\rho d)_{\rm Xe}$	$n(\mu\rho d)_{\rm P}\Delta E/E$	$R_{\rm calc}$	$R_{\rm meas}$
5	8	−0.0818	0.0026	−0.0792	−0.051
4	9	−0.0654	0.0029	−0.0625	−0.039
3	10	−0.049	0.0032	−0.0458	−0.0301
2	11	−0.0327	0.0036	−0.0291	−0.0208
1	12	−0.0164	0.0039	−0.0125	−0.0112
0.5	12.5	−0.0082	0.004	−0.0042	–

(i) the phantom cavity was not completely evacuated of air before it was filled with xenon, and therefore a mixture of xenon and air were in the phantom during the experiments; (ii) differences between the theoretical and experimental values of constants n and $\Delta E/E$.

A 1 mm thickness of Plexiglass decreases the photon flux by 3.1%. The corresponding values for xenon are 0.35% at the energy below the *K*-absorption edge and 1.98% at the energy above the *K*-edge. This means that crossing from one step of the phantom to the adjoining one with an increase of 1 mm thickness of xenon must provide a 1.63% increase in the subtraction signal. The measured value is about 1.1%.

Fig. 3 shows the X-ray images of the phantom. The left-hand and middle images are the usual X-ray images at energies above and below the xenon *K*-edge, respectively. Shown in these two images are the monochromatic beams without the phantom (white horizontal strips on the top of the images), the absorption in the Plexiglass only (black horizontal strips just under the top white strips), and the five series of strips corresponding to the absorption in different thicknesses of xenon of 5 (top), 4, 3, 2 and 1 mm (bottom). The image contrast of the middle picture (below the *K*-edge) is slightly better than that of the left-hand image (above the *K*-edge). This effect can be explained by the design of the phantom. In passing from one phantom step to the next step, the thickness of Plexiglass increases by 1 mm and the thickness of the xenon layer decreases by 1 mm simultaneously. The coefficient of the photon absorption increases by 3.1% due to absorption in Plexiglass and decreases by 0.35% below and by 1.98% above the *K*-edge energy, respectively. As a result, at the energy below the *K*-edge of xenon the total absorption in the phantom changes by the value $3.1 - 0.35 = 2.75\%$, and at the energy above the *K*-edge of xenon the total absorption changes by the value $3.1 - 1.98 = 1.12\%$. This difference explains the difference in the image contrast between the usual X-ray images at the energies below and above the *K*-edge of xenon.

The right-hand image is different, visualizing five steps of xenon thickness from 5 mm down to 1 mm. The right-hand part of Fig. 3 shows the xenon distribution curve in the phantom along the vertical direction. As may be seen, a 1 mm thickness of xenon is easy visualized. A comparison between the level of noise and the value of the 1 mm Xe thickness step signal on the xenon distribution curve allows us to expect that a 0.5 mm thickness of xenon must also be detected.

4. Conclusions

The experiments have demonstrated that the existing angiography station of the VEPP-3, designed originally for angiography studies at the iodine *K*-absorption edge, can also be applied for bronchography studies at the Xe *K*-edge. The obtained preliminary results with the phantom show that a 1 mm thickness of xenon is

reliably visualized. It can also be expected, according to the results, that a 0.5 mm xenon thickness can be detected.

References

Barsukov, V. P., Dolbnya, I. P., Kolokolnikov, Yu. M., Kurylo, S. G., Mezentsev, N. A., Pindyurin, V. F. & Sheromov, M. A. (1991). *Nucl. Instrum. Methods*, A**308**, 419–422.

Dementiev, E. N., Dolbnya, I. P., Zagorodnikov, E. I., Kolesnikov, K. A., Kulipanov, G. N., Kurylo, S. G., Medvedko, A. S., Mezentsev, N. A., Pindyurin, V. F., Cheskidov, V. G. & Sheromov, M. A. (1989). *Rev. Sci. Instrum.* **60**(7), 2264–2267.

Kolesnikov, K. A., Kozlov, R. Yu., Kulipanov, G. N., Kuzin, M. V., Mezentsev, N. A., Nesterov, S. I., Pindyurin, V. F., Dragun, G. N., Zelentsov, E. L. & Rozenberg, O. (1996). *Proceedings of the 4th International Conference on Synchrotron Radiation Sources and 2nd Asian Forum on Synchrotron Radiation: ICSRS-AFSR'95*, edited by M. Yoon & S. H. Nam, pp. 543–552. Pohang, Kyungbuk: PAL, POSTECH.

Kolesnikov, K. A., Kulipanov, G. N., Kuzin, M. V., Mezentsev, N. A., Nesterov, S. I., Pindyurin, V. F., Dragun, G. N., Zelentsov, E. L. & Rozenberg, O. (1995). *Nucl. Instrum. Methods*, A**359**, 364–369.

Rubenstein, E., Giacomini, J. C., Gordon, H. J., Rubenstein, J. A. L. & Broun, G. (1995). *Nucl. Instrum. Methods*, A**364**, 360–361.

Zapisov, A. L., Ganeev, A. S., Izrailev, I. M., Savin, N. I. & Saprykin, V. N. (1975). *X-ray Absorption Coefficients.* Leningrad: LNPO. (In Russian.)